Wavepacket instability in a rectangular porous channel uniformly heated from below

# Wavepacket instability in a rectangular porous channel uniformly heated from below

**A. Barletta[+*] , M. Celli[+], P. Vayssiere Brandão[+], L. S. de B. Alves[°]**

[+] ***Alma Mater Studiorum Università di Bologna,***
***Department of Industrial Engineering,***
***Viale Risorgimento, 2 – 40136 Bologna, Italy***

[°] ***Universidade Federal Fluminense,***
***Departamento de Engenharia Mecânica,***
***Rua Passo da Pátria 156, bloco E, sala 211 – Niterói, RJ 24210-240, Brazil***

**Abstract**

This paper is aimed to investigate the transition to absolute instability in a porous layer with horizontal throughflow. The importance of this analysis is due to the possible experimental failure to detect growing perturbations which are localised in space and which may be convected away by the throughflow. The instability of the uniform flow in a horizontal rectangular channel subject to uniform heating from below and cooled from above is studied. While the lower wall is modelled as an impermeable isoflux plane, the upper wall is assumed to be impermeable and imperfectly conducting, so that a Robin temperature condition with a given finite Biot number is prescribed. The sidewalls are assumed to be adiabatic and impermeable. The basic state under exam is a stationary parallel flow with a vertical uniform temperature gradient, namely the typical configuration describing the Darcy–Bénard instability with throughflow. The linear instability of localised wavepackets is analysed, thus detecting the parametric conditions for the transition to absolute instability. The absolute instability problem is formulated through an eigenvalue problem based on an eighth–order system of ordinary differential equations. The solution is sought numerically by utilising the shooting method. The threshold to absolute instability is detected versus the Péclet number associated with the basic flow rate along the channel.

**Key Words:** Rectangular porous channel; Mixed convection; Darcy–Bénard instability; Uniform wall heat flux; Biot number; Linear wavepackets; Absolute instability

*Corresponding author, Email: antonio.barletta@unibo.it

**Nomenclature**

| | |
|---|---|
| $A$ | aspect ratio, Eq. (3) |
| $\mathcal{A}_n$ | function, Eq. (20) |
| $B$ | Biot number, Eq. (3) |
| $\mathcal{B}_n$ | function, Eq. (20) |
| $\boldsymbol{e}_z$ | unit vector in the $z$–direction |
| $f$ | function, Eq. (16) |
| $F$ | rescaled function $f$, Eq. (42) |
| $\mathcal{F}$ | function defined by Eq. (52) |
| $g$ | modulus of gravitational acceleration |
| $h$ | function, Eq. (16) |
| $H$ | channel height |
| $\mathcal{H}$ | adjoint of $h$ employed in Eq. (53) |
| $k$ | wavenumber |
| $K$ | permeability of the porous layer |
| $P$ | Péclet number, Eq. (5) |
| $q_0$ | constant wall heat flux |
| $r_1, r_2$ | dimensionless parameters, Eq. (38e) |
| $R$ | Darcy–Rayleigh number, Eq. (3) |
| $s$ | dimensionless parameter, Eq. (35) |
| $t$ | time |
| $T$ | temperature |
| $\hat{T}_n$ | Fourier series coefficients, Eq. (10) |
| $T_0$ | reference temperature |
| $\boldsymbol{u}$ | velocity vector, $(u, v, w)$ |
| $\boldsymbol{x}$ | position vector, $(x, y, z)$ |

*Greek symbols*

| | |
|---|---|
| $\alpha$ | rescaled wavenumber, Eq. (25) |
| $\beta$ | thermal expansion coefficient of the fluid |
| $\gamma$ | external heat transfer coefficient |
| $\varepsilon$ | dimensionless perturbation amplitude parameter, Eq. (6) |
| $\zeta_1, \zeta_2$ | dimensionless parameters, Eq. (29) |
| $\eta$ | perturbation growth rate, Eq. (23) |
| $\hat{\Theta}_n$ | Fourier transforms, Eq. (12) |
| $\varkappa$ | average thermal diffusivity |
| $\lambda$ | function of $k$, Eq. (16) |
| $\Lambda$ | rescaled $\lambda$, Eq. (42) |
| $\mu$ | dynamic viscosity |
| $\xi$ | heat capacity ratio |
| $\rho$ | reference density of the fluid |
| $\tau$ | rescaled Darcy–Rayleigh number $R$, Eq. (42) |
| $\phi$ | scalar field, Eq. (8) |
| $\hat{\phi}_n$ | Fourier series coefficients, Eq. (10) |
| $\hat{\Phi}_n$ | Fourier transforms, Eq. (12) |

| | |
|---|---|
| $\chi$ | average thermal conductivity of the porous medium |
| $\hat{\Psi}_n$ | functions, Eq. (14) |
| $\omega$ | perturbation angular frequency, Eq. (23) |

*Superscript, Subscripts*

| | |
|---|---|
| $a$ | absolute instability threshold value |
| $b$ | basic state, Eq. (5) |
| $c$ | critical value |
| $^-$ | complex conjugate |
| $\hat{}$ | perturbations, Eq. (6) |
| $\tilde{}$ | derivative with respect to $k$, Eq. (33) |
| $'$ | derivative with respect to $z$ |

## 1. Introduction

The usual analysis of linear thermal instability in a horizontal porous channel regards the response of the basic flow to normal mode perturbations [1, 2]. In other words, the growth or decay in time of planar wave perturbations travelling along the channel is recorded to detect the threshold of linear instability and the critical parameters triggering its onset. In practical cases, the natural disturbances perturbing the flow are more realistically modelled as wavepackets well localised in space and driven by the basic flow. When the focus is on the emergence of wavepacket perturbations ultimately growing in time at given spatial positions, one detects the parametric threshold to absolute instability. This terminology serves to mark the difference with the usual instability versus normal modes of perturbation, usually called convective instability. The threshold to absolute instability, in fact, generally belongs to a supercritical domain where the order parameter driving the instability is larger than its critical value. There exist many surveys describing the concept of absolutely unstable situations regarding either plasma physics, fluid mechanics, or more general diffusion phenomena [3–12]. A couple of them focus on some classical, and also propose novel, numerical techniques to deal with these situations [13, 14]. A recent book supplied a pedagogical introduction to this topic specifically oriented to convection flows in porous media [15].

The onset of a Rayleigh–Bénard instability in a horizontal porous layer saturated by a fluid is a classical problem first addressed in the pioneering papers by Horton and Rogers [16], and Lapwood [17]. The main information gathered with these studies is that the critical value of the Darcy–Rayleigh number for the onset of convective instability is $4\,\pi^2$, when the plane horizontal boundaries are isothermal. The Darcy–Rayleigh number, $R$, is the porous medium version of the Rayleigh number, employed for a fluid, which involves the permeability of the medium. The critical value of $R$ is reduced to 27.1 if one of the two boundary walls is isoflux instead of isothermal. Later on, Prats [1] studied the effect of a horizontal throughflow in the channel parametrised by the Péclet number. Nowadays, it is commonly used the term Prats problem to denote the situation envisaged in that paper. Prats [1] proved that the Péclet number turns out to be ineffective in changing the critical value of the Darcy–Rayleigh number for the linear instability. Its only effect is the travelling nature of the normal modes triggering the instability, with a phase velocity induced by the basic flow rate.

When the analysis shifts from the assessment of the convective instability in porous media to the study of the transition to absolute instability, the literature is definitely more recent [18–25]. This paper aims to contribute to the existing literature with the analysis of the absolute instability for a flow condition similar to that described with the Prats problem. The differences regard the temperature boundary

conditions. In the next sections, we will be interested in a flow regime where the lower boundary is heated with a uniform heat flux, while the temperature is subjected to Robin conditions at the upper boundary. This means that the upper boundary exchanges heat with an external environment through a finite heat transfer coefficient or, in dimensionless terms, a finite Biot number. The dynamics of wavepacket perturbations at large times will be studied numerically by employing the steepest–descent approximation. Thus, the threshold of absolute instability will be detected for different Biot numbers and Péclet numbers.

## 2. Mathematical model

Let us consider a horizontal porous channel having a rectangular cross-section with height $H$ and spanwise width $L$. The coordinates are chosen so that $x$ is the longitudinal horizontal axis and $y$ is the spanwise horizontal axis, while the $z$ axis is vertical (see Fig. 1). While the system is confined in the $y$ and $z$ directions, there is no bounding plane in the $x$ direction or, equivalently, the system is infinitely wide in the $x$ direction.

The velocity field $\boldsymbol{u} = (u, v, w)$ and the temperature field $T$, as well as the position vector $\boldsymbol{x} = (x, y, z)$ and time $t$, can be written in a dimensionless form by adopting the following transformation

$$\begin{aligned} &\boldsymbol{u}\,\frac{H}{\varkappa} = (u, v, w)\,\frac{H}{\varkappa} = (u^*, v^*, w^*) = \boldsymbol{u}^*, \qquad (T - T_0)\,\frac{\chi}{q_0 H} = T^*, \\ &\boldsymbol{x}\,\frac{1}{H} = (x, y, z)\,\frac{1}{H} = (x^*, y^*, z^*) = \boldsymbol{x}^*, \qquad t\,\frac{\varkappa}{H^2} = t^*. \end{aligned} \tag{1}$$

Here, the asterisks denote dimensionless quantities, while $\varkappa$ is the average thermal diffusivity and $\chi$ is the average thermal conductivity of the porous medium, while $q_0$ is the constant wall heat flux imposed on the lower boundary of the channel, while $T_0$ is the constant temperature of the upper fluid environment.

Hereafter, we will drop the asterisks in the dimensionless quantities as their dimensional counterparts will not be involved anymore. According to the Oberbeck-Boussinesq approximation and Darcy's law, the dimensionless governing equations expressing the local balances of mass, momentum and energy can be written as

$$\boldsymbol{\nabla} \cdot \boldsymbol{u} = 0, \tag{2a}$$

$$\boldsymbol{\nabla} \times \boldsymbol{u} = R\,\boldsymbol{\nabla} \times (T\boldsymbol{e}_z)\,, \tag{2b}$$

$$\xi\,\frac{\partial T}{\partial t} + \boldsymbol{u} \cdot \boldsymbol{\nabla} T = \nabla^2 T, \tag{2c}$$

where $\boldsymbol{e}_z$ is the unit vector along the $z$ axis, and the local momentum balance (2b) has been expressed in its vorticity formulation. The parameter $\xi$ is the ratio between the average volumetric heat capacity of the saturated porous medium and the volumetric heat capacity of the fluid. The Darcy-Rayleigh number $R$, the Biot number, $B$, and the aspect ratio $A$ are defined as

$$R = \frac{\rho g \beta q_0 K\, H^2}{\mu \varkappa \chi}, \qquad B = \frac{\gamma H}{\chi}, \qquad A = \frac{L}{H}, \tag{3}$$

where $\beta$ is the thermal expansion coefficient of the fluid, $g$ is the modulus of the gravitational acceleration, $K$ is the permeability, $\mu$ is the dynamic viscosity of the fluid, $\rho$ is the reference fluid density, and $\gamma$ is the heat transfer coefficient to the external fluid environment.

Conditions are imposed in order to model the vertical impermeable and adiabatic sidewalls, as well as the impermeable and isoflux horizontal walls, $z = 0$ and $z = 1$,

$$y = 0, A \;: \qquad v = 0, \quad \frac{\partial T}{\partial y} = 0, \tag{4a}$$

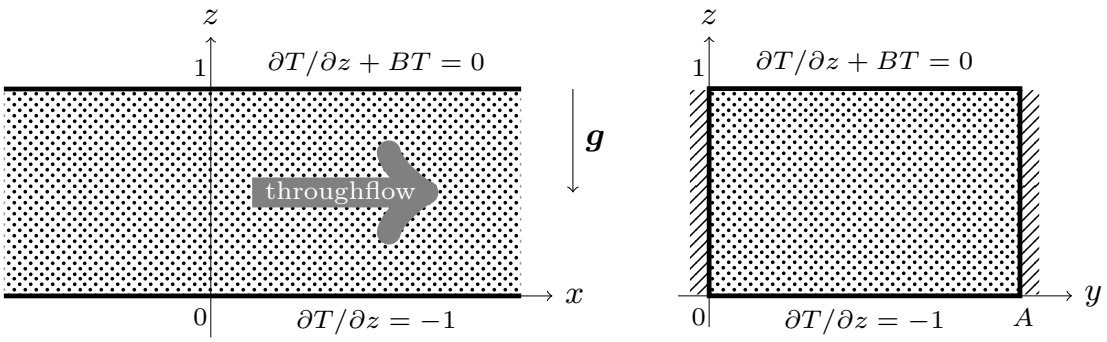


Figure 1: A sketch of the porous channel

$$z = 0 \ : \qquad w = 0, \quad \frac{\partial T}{\partial z} = -1, \tag{4b}$$

$$z = 1 \ : \qquad w = 0, \quad \frac{\partial T}{\partial z} + BT = 0. \tag{4c}$$

*2.1. Basic throughflow solution*

A stationary solution of Eqs. (2) satisfying the boundary conditions (4), which describes a parallel throughflow in the $x-$direction, is given by

$$\boldsymbol{u}_b = (u_b, v_b, w_b) = (P, 0, 0), \qquad T_b = \frac{B+1}{B} - z, \tag{5}$$

where the dimensionless parameter $P$ plays the role of the Péclet number associated with the basic horizontal throughflow.

## 3. Linearised perturbation equations

We can express small–amplitude perturbations to the basic solution as

$$\boldsymbol{u} = \boldsymbol{u}_b + \varepsilon \hat{\boldsymbol{u}}, \qquad T = T_b + \varepsilon \hat{T}, \tag{6}$$

where $\hat{\boldsymbol{u}} = (\hat{u}, \hat{v}, \hat{w})$ and $\hat{T}$ are the velocity and temperature disturbances, respectively, while $\varepsilon$ is a perturbation amplitude such that $|\varepsilon| \ll 1$.

Since the basic solution (5) satisfies Eqs. (2) and (4), the substitution of Eq. (6) into Eqs. (2) and (4), upon neglecting terms $O(\varepsilon^2)$, yields

$$\boldsymbol{\nabla} \cdot \hat{\boldsymbol{u}} = 0, \tag{7a}$$

$$\boldsymbol{\nabla} \times \left( \hat{\boldsymbol{u}} - R\hat{T}\,\boldsymbol{e}_z \right) = 0, \tag{7b}$$

$$\xi \frac{\partial \hat{T}}{\partial t} + P \frac{\partial \hat{T}}{\partial x} - \hat{w} = \nabla^2 \hat{T}, \tag{7c}$$

$$y = 0, A \ : \qquad \hat{v} = 0, \quad \frac{\partial \hat{T}}{\partial y} = 0, \tag{7d}$$

$$z = 0 \ : \qquad \hat{w} = 0, \quad \frac{\partial \hat{T}}{\partial z} = 0, \tag{7e}$$

$$z = 1 \ : \qquad \hat{w} = 0, \quad \frac{\partial \hat{T}}{\partial z} + B\hat{T} = 0. \tag{7f}$$

We now adopt a pressure formulation by defining a scalar field $\hat{\phi}$ such that

$$\hat{\boldsymbol{u}} - R\hat{T}\boldsymbol{e}_z = -\boldsymbol{\nabla}\hat{\phi}. \tag{8}$$

With Eq. (8), Eq. (7b) is identically satisfied, while Eqs. (7a), (7c), (7d) and (7e) can be rewritten as

$$\nabla^2\hat{\phi} = R\,\frac{\partial\hat{T}}{\partial z}, \tag{9a}$$

$$\nabla^2\hat{T} = \xi\,\frac{\partial\hat{T}}{\partial t} + P\,\frac{\partial\hat{T}}{\partial x} + \frac{\partial\hat{\phi}}{\partial z} - R\,\hat{T}, \tag{9b}$$

$$y = 0, A \;:\quad \frac{\partial\hat{\phi}}{\partial y} = 0, \quad \frac{\partial\hat{T}}{\partial y} = 0, \tag{9c}$$

$$z = 0 \;:\quad \frac{\partial\hat{\phi}}{\partial z} = R\,\hat{T}, \quad \frac{\partial\hat{T}}{\partial z} = 0, \tag{9d}$$

$$z = 1 \;:\quad \frac{\partial\hat{\phi}}{\partial z} = R\,\hat{T}, \quad \frac{\partial\hat{T}}{\partial z} + B\hat{T} = 0. \tag{9e}$$

### *3.1. Normal modes*

Due to the linearity and to the boundary conditions (9c)–(9e), the solution of Eqs. (9) can be sought by expressing $\hat{\phi}$ and $\hat{T}$ as Fourier series with respect to $y$ [26],

$$\begin{aligned}\hat{\phi}(x,y,z,t) &= \sum_{n=0}^{\infty}\hat{\phi}_n(x,z,t)\cos(n\pi y/A),\\ \hat{T}(x,y,z,t) &= \sum_{n=0}^{\infty}\hat{T}_n(x,z,t)\cos(n\pi y/A).\end{aligned} \tag{10}$$

As a consequence, Eqs. (9) can be rewritten as

$$\nabla_2^2\hat{\phi}_n - \frac{n^2\pi^2}{A^2}\,\hat{\phi}_n = R\,\frac{\partial\hat{T}_n}{\partial z}, \tag{11a}$$

$$\nabla_2^2\hat{T}_n - \frac{n^2\pi^2}{A^2}\,\hat{T}_n = \xi\,\frac{\partial\hat{T}_n}{\partial t} + P\,\frac{\partial\hat{T}_n}{\partial x} + \frac{\partial\hat{\phi}_n}{\partial z} - R\,\hat{T}_n, \tag{11b}$$

$$z = 0 \;:\quad \frac{\partial\hat{\phi}_n}{\partial z} = R\,\hat{T}_n, \quad \frac{\partial\hat{T}_n}{\partial z} = 0, \tag{11c}$$

$$z = 1 \;:\quad \frac{\partial\hat{\phi}_n}{\partial z} = R\,\hat{T}_n, \quad \frac{\partial\hat{T}_n}{\partial z} + B\,\hat{T}_n = 0, \tag{11d}$$

where $n = 0, 1, 2, \dots$, and $\nabla_2^2 = \partial^2/\partial x^2 + \partial^2/\partial z^2$ is the two-dimensional Laplacian operator. We now express $\hat{\phi}_n$ and $\hat{T}_n$ through their Fourier transforms with respect to $x$ [26],

$$\hat{\Phi}_n(z,t,k) = \frac{1}{\sqrt{2\pi}}\int_{-\infty}^{\infty} e^{-ikx}\,\hat{\phi}_n(x,z,t)\,dx, \tag{12a}$$

$$\hat{\Theta}_n(z,t,k) = \frac{1}{\sqrt{2\pi}}\int_{-\infty}^{\infty} e^{-ikx}\,\hat{T}_n(x,z,t)\,dx. \tag{12b}$$

As a consequence of Eqs. (12), Eqs. (11) can be rewritten as

$$\frac{\partial^2\hat{\Phi}_n}{\partial z^2} - \left(k^2 + \frac{n^2\pi^2}{A^2}\right)\hat{\Phi}_n = R\,\frac{\partial\hat{\Theta}_n}{\partial z}, \tag{13a}$$

$$\frac{\partial^2\hat{\Theta}_n}{\partial z^2} - \left(k^2 + \frac{n^2\pi^2}{A^2}\right)\hat{\Theta}_n = \xi\,\frac{\partial\hat{\Theta}_n}{\partial t} + ikP\,\hat{\Theta}_n + \frac{\partial\hat{\Phi}_n}{\partial z} - R\,\hat{\Theta}_n, \tag{13b}$$

$$z = 0 \;:\quad \frac{\partial\hat{\Phi}_n}{\partial z} = R\,\hat{\Theta}_n, \quad \frac{\partial\hat{\Theta}_n}{\partial z} = 0, \tag{13c}$$

$$z = 1 \;:\quad \frac{\partial\hat{\Phi}_n}{\partial z} = R\,\hat{\Theta}_n, \quad \frac{\partial\hat{\Theta}_n}{\partial z} + B\,\hat{\Theta}_n = 0. \tag{13d}$$

A simpler reformulation of the boundary value problem (13) is given in terms of function $\hat{\Psi}_n$, defined as

$$\hat{\Psi}_n = \frac{\partial \hat{\Phi}_n}{\partial z} - R\,\hat{\Theta}_n, \tag{14}$$

employed to remove the coupling between $\hat{\Phi}_n$ and $\hat{\Theta}_n$ in the boundary conditions at $z = 0$ and $z = 1$, yielding

$$\frac{\partial^2 \hat{\Psi}_n}{\partial z^2} - \left(k^2 + \frac{n^2\pi^2}{A^2}\right)\left(\hat{\Psi}_n + R\,\hat{\Theta}_n\right) = 0, \tag{15a}$$

$$\frac{\partial^2 \hat{\Theta}_n}{\partial z^2} - \xi\,\frac{\partial \hat{\Theta}_n}{\partial t} - \left(k^2 + \frac{n^2\pi^2}{A^2} + ikP\right)\hat{\Theta}_n - \hat{\Psi}_n = 0, \tag{15b}$$

$$z = 0 \;:\qquad \hat{\Psi}_n = 0, \quad \frac{\partial \hat{\Theta}_n}{\partial z} = 0, \tag{15c}$$

$$z = 1 \;:\qquad \hat{\Psi}_n = 0, \quad \frac{\partial \hat{\Theta}_n}{\partial z} + B\,\hat{\Theta}_n = 0. \tag{15d}$$

The eigenvalue problem (15) can be solved by separation of variables, *i.e.* by factoring out the dependences on time and vertical coordinate. We use

$$\hat{\Psi}_n(z,t,k) = e^{\lambda(k)\,t/\xi}\,f(z), \qquad \hat{\Theta}_n(z,t,k) = e^{\lambda(k)\,t/\xi}\,h(z), \tag{16}$$

where $f(z)$ and $h(z)$ depend also on $k$ and $n$, although not made explicit in the notation for the sake of brevity. On account of Eq. (16), we can express Eqs. (15) as an ordinary differential problem,

$$f'' - \left(k^2 + \frac{n^2\pi^2}{A^2}\right)(f + R\,h) = 0, \tag{17a}$$

$$h'' - \lambda(k)\,h - \left(k^2 + \frac{n^2\pi^2}{A^2} + ikP\right)h - f = 0, \tag{17b}$$

$$z = 0 \;:\qquad f = 0, \quad h' = 0, \tag{17c}$$

$$z = 1 \;:\qquad f = 0, \quad h' + Bh = 0. \tag{17d}$$

### *3.2. Wavepacket dynamics and absolute instability*

If one employs the inversion formula of Fourier transforms [26], as well as Eqs. (12), (14) and (16), one obtains the expressions

$$\hat{\psi}_n(x,z,t) = \frac{1}{\sqrt{2\pi}}\int_{-\infty}^{\infty} e^{ikx}\,e^{\lambda(k)\,t/\xi}\,f(z)\,dk, \tag{18a}$$

$$\hat{T}_n(x,z,t) = \frac{1}{\sqrt{2\pi}}\int_{-\infty}^{\infty} e^{ikx}\,e^{\lambda(k)\,t/\xi}\,h(z)\,dk. \tag{18b}$$

Here, $\hat{\psi}_n(x,z,t)$ denotes the inverse Fourier transform of $\hat{\Psi}_n(z,t,k)$. We recall that the latter function is defined through Eq. (14). Equation (18) highlights the structures of the perturbations as wavepackets given by the envelope of Fourier normal modes endowed with a single wavenumber $k$,

$$\frac{1}{\sqrt{2\pi}}\,e^{ikx}\,e^{\lambda(k)\,t/\xi}\,f(z), \qquad \frac{1}{\sqrt{2\pi}}\,e^{ikx}\,e^{\lambda(k)\,t/\xi}\,h(z). \tag{19}$$

If there exists at least one wavenumber, $k$, such that $\mathfrak{Re}(\lambda(k)) > 0$, then this normal mode will be growing in time. If such a situation happens, we call it *convective instability*. It is the usual sense of linear instability intended as the response of the basic flow to a single Fourier normal mode. As such, the convective instability is a wavenumber–dependent condition resulting into a threshold, the neutral

stability curve, where the Darcy–Rayleigh number, $R$, yielding the onset of instability is traced by varying $k$. The smallest $R$ along the neutral stability curve is the critical value, $R_c$, usually endowed with the physical meaning of the upper limit for flow stability. The corresponding wavenumber is the critical value, $k_c$.

Another approach to the definition of unstable behaviour is one based on the response of the basic flow to a wavepacket perturbation. Here, each individual normal mode with a given $k$ is not singled out, but the effects of the continuous superposition of all possible normal modes expressed through the integrals employed in Eqs. (18) is accounted for. In this case, the instability has a $k$–independent nature and it is termed *absolute instability*. The threshold to absolute instability, expressed in terms of the Darcy–Rayleigh number, happens with $R = R_a \geqslant R_c$. The equal sign may occur when the net flow rate associated with the basic solution vanishes, *i.e.*, $R_a = R_c$. On the other hand, generally speaking, there is a gap between the thresholds of convective and absolute instability, $R_a > R_c$, when the net flow rate is nonzero.

Given that the transition to convective instability means determining which value of $R$ yields the marginal condition $\mathfrak{Re}(\lambda(k)) = 0$, the analysis of the transition to absolute instability requires some more effort. One must detect which value of $R$ changes the limits as $t \to +\infty$ of $|\hat{\psi}_n(x,z,t)|$ and $|\hat{T}_n(x,z,t)|$ from $\infty$ to 0. The first consideration is that such a value of $R$ does the job for both the amplitudes $|\hat{\psi}_n(x,z,t)|$ and $|\hat{T}_n(x,z,t)|$. This means that their limits switch from $\infty$ to 0 for the same threshold value of the Darcy–Rayleigh number, $R_a$. This is a consequence of the steepest–descent approximation [15, 27, 28] when applied to $|\hat{\psi}_n(x,z,t)|$ and $|\hat{T}_n(x,z,t)|$, for large values of $t$,

$$|\hat{\psi}_n(x,z,t)| \simeq \frac{\mathcal{A}_n(x,z)}{\sqrt{t}}\, e^{\,\mathfrak{Re}(\lambda(k_0))\,t/\xi}, \qquad |\hat{T}_n(x,z,t)| \simeq \frac{\mathcal{B}_n(x,z)}{\sqrt{t}}\, e^{\,\mathfrak{Re}(\lambda(k_0))\,t/\xi}. \tag{20}$$

Here, functions $\mathcal{A}_n(x,z)$ and $\mathcal{B}_n(x,z)$ are independent of time and $k_0$ is a saddle point, namely a solution of equation

$$\lambda'(k) = 0, \tag{21}$$

to be determined in the complex plane, $k \in \mathbb{C}$. On account of Eq. (20), whether $|\hat{\psi}_n(x,z,t)|$ and $|\hat{T}_n(x,z,t)|$ tend to $\infty$ or 0 as $t \to +\infty$ depends on $\mathfrak{Re}(\lambda(k_0))$ being positive, zero or negative. When $\mathfrak{Re}(\lambda(k_0))$ is negative or zero, both $|\hat{\psi}_n(x,z,t)|$ and $|\hat{T}_n(x,z,t)|$ tend to zero. When $\mathfrak{Re}(\lambda(k_0))$ is positive, both $|\hat{\psi}_n(x,z,t)|$ and $|\hat{T}_n(x,z,t)|$ tend to infinity. Then, it is clear that the threshold condition for absolute instability is

$$\mathfrak{Re}(\lambda(k_0)) = 0. \tag{22}$$

There is an assumption behind the scenes, namely the *holomorphy requirement* [15] asking that the integrands appearing at the right–hand sides of Eqs. (18) do not have any singularity in the region of the complex $k$ plane bounded by the real axis, $k \in \mathbb{R}$, and by a path crossing the saddle point $k_0$ which is, locally, of steepest descent for $\mathfrak{Re}(\lambda(k))$. The latter feature implies that, along this path, $\mathfrak{Re}(\lambda(k))$ becomes negative at its highest possible rate on departing from $k_0$. Equation (20), together with the above reasoning, justifies the anticipated unambiguous nature of the threshold $R_a$ as Eqs. (21) and (22) refer either to $|\hat{\psi}_n(x,z,t)|$ or to $|\hat{T}_n(x,z,t)|$. Another important feature of the absolute instability is that it relies only on the properties of function $\lambda(k)$. Thus, it is independent of any detail about the shape of the perturbation wavepackets inasmuch as their features do not prevent the validity of the holomorphy requirement. We refer the reader to Barletta [15] for further details and examples.

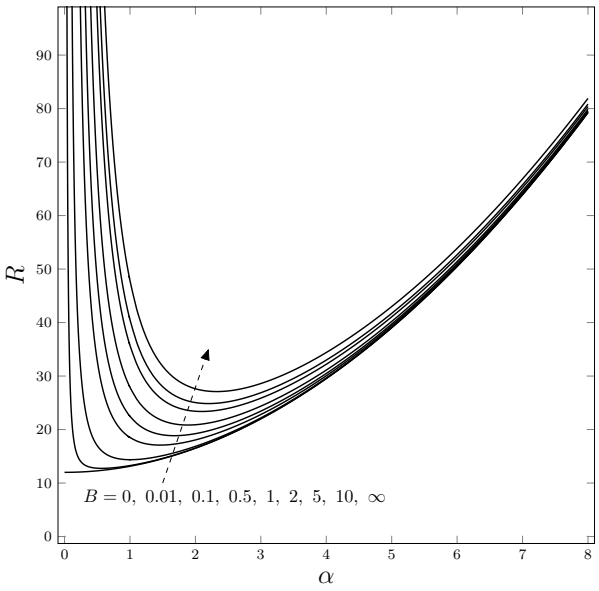


Figure 2: Neutral stability curves $R$ versus $\alpha$

## 4. Numerical analysis of the instability

The numerical solution of Eqs. (17) can be obtained in different ways depending on our interest in detecting the thresholds to either convective or absolute instability.

### *4.1. Neutral stability or the onset of convective instability*

If the aim is determining the onset of convective instability, then we are interested in obtaining the neutral stability condition. We define the real and the imaginary parts of $\lambda(k)$, so that

$$\lambda = \eta - i\xi\omega. \tag{23}$$

An important result is the principle of exchange of stabilities [29] when applied to the co-moving reference frame, which means

$$\xi\omega - kP = 0. \tag{24}$$

The proof of this result for the flow under exam can be found, for instance, in Alves and Barletta [30]. Furthermore, if we define

$$\alpha^2 = k^2 + \frac{n^2\pi^2}{A^2}, \tag{25}$$

Eqs. (17) can be drastically simplified

$$f'' - \alpha^2 (f + R\, h) = 0, \tag{26a}$$

$$h'' - \left(\eta + \alpha^2\right) h - f = 0, \tag{26b}$$

$$z = 0 \ : \qquad f = 0, \quad h' = 0, \tag{26c}$$

$$z = 1 \ : \qquad f = 0, \quad h' + Bh = 0. \tag{26d}$$

Equations (26) can be solved as an eigenvalue problem to determine the neutral stability condition, $\eta = 0$. In this case, $R$ is the eigenvalue to be traced versus the parameter $\alpha$, for any prescribed value of $B$. This representation of the neutral stability condition is provided in Fig. 2.

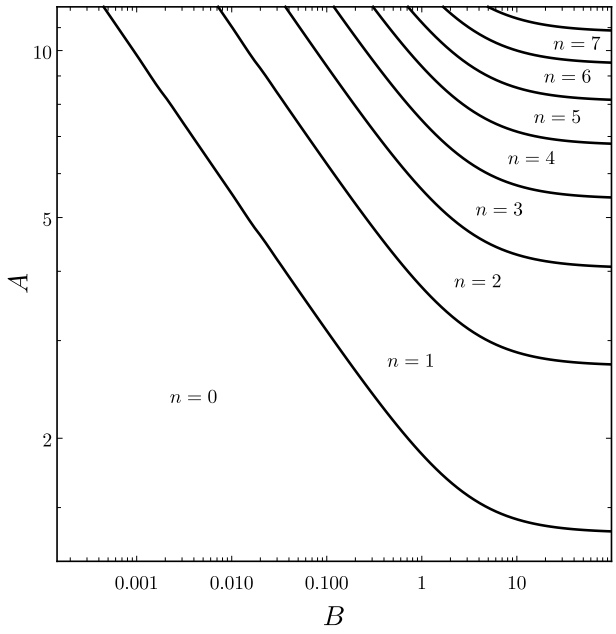


Figure 3: Distribution, in the $(B, A)$ plane, of the multiplicity of modes $(k, n)$ corresponding to $\alpha = \alpha_c$

The numerical solution of Eqs. (26) with $\eta = 0$ is accomplished by employing the shooting method. This technique is based on the reformulation of Eqs. (26) as an initial value problem based at $z = 0$, with the definition of a suitable dummy parameter. Then, the initial value problem is solved by a fourth–order Runge–Kutta method and the dummy parameter, together with the eigenvalue, is computed by a root finding algorithm to fit the end boundary conditions prescribed at $z = 1$. This very accurate procedure is described in detail by Straughan [31] and by Barletta [15]. The mentioned eigenvalue is, in fact, the Darcy–Rayleigh number, $R$, which can be computed for every assignment of the pair of input data, $(\alpha, B)$.

Different values of $B$ are considered in Fig. 2, and the limiting cases of either isothermal ($B \to \infty$) or isoflux ($B \to 0$) upper boundary are represented for comparison. An increasing Biot number results into a stabilisation of the basic flow, as it produces an upward drift of the neutral stability curve, so that convective instability happens with gradually increasing values of $R$.

The same $\alpha$ can be determined by different pairs $(k, n)$, that is different normal modes triggering the onset of instability. Which modes and how many of them are involved in the critical condition $(\alpha_c, R_c)$, for a given $B$, can be established by employing Eq. (25). An exception where the critical mode is unique is given by the limiting case $B \to 0$. As sketched in Fig. 2 and well–known from the literature [2], the limiting case $B \to 0$ yields $\alpha_c = 0$, which means that there is just one critical mode, $(k = 0, n = 0)$. With a nonzero $B$, things are different as $\alpha_c \neq 0$.

Figure 3 illustrates how the multiplicity of modes determining the critical condition $(\alpha_c, R_c)$, for a given $B$, depends on the aspect ratio $A$. For instance, the strip region denoted with $n = 2$ indicates the parametric condition where only the modes with $n = 0, 1, 2$ are possible critical modes with a suitable $k_c$ determined by Eq. (25), while no mode with $n > 2$ is allowed. The geometry of the strip regions with different $n$ suggests that, in the limit $B \to 0$, only the $n = 0$ mode may trigger the convective instability, as already pointed out above. Moreover, one may see that, as $B$ increases, the multiplicity of modes is mainly influenced by the aspect ratio $A$ with a weaker and weaker dependence on $B$. The rough conclusion gathered from Fig. 3 is that the multiplicity of modes associated with the critical condition increases with the aspect ratio $A$, the shallower is the channel cross–section the higher is the number of allowed modes yielding $\alpha = \alpha_c$.

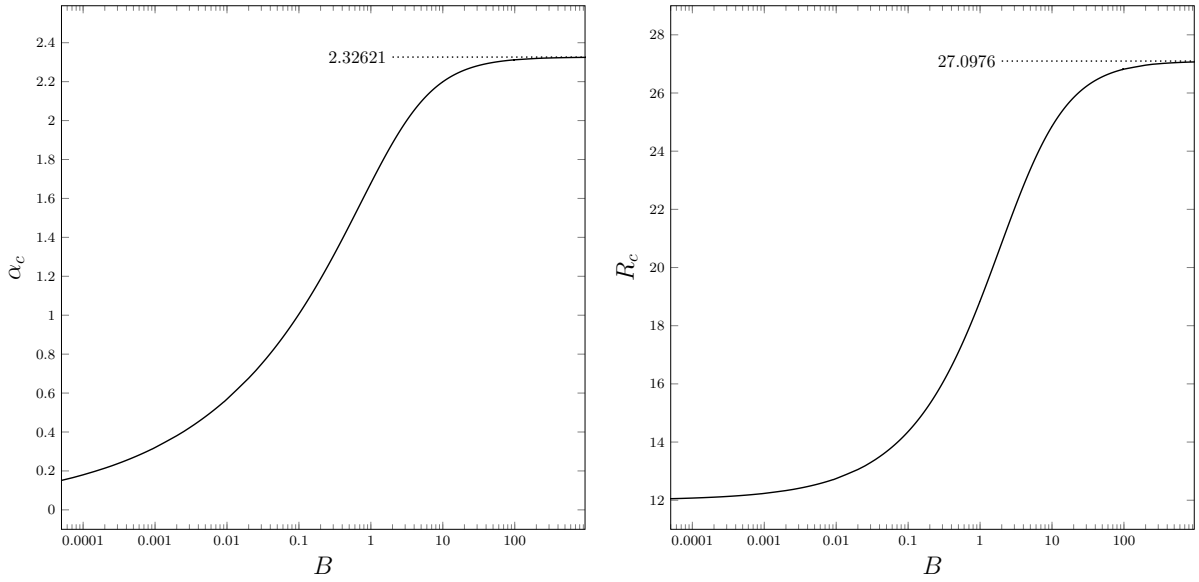


Figure 4: Critical values of $\alpha$ and $R$ versus $B$

| $B$ | $R$ |
|---|---|
| 10 | 40.5160456757317 |
| 1 | 22.4699539020801 |
| 0.1 | 14.3608848310611 |
| 0.01 | 13.2645032654520 |

Table 1: Neutral stability values of $R$ versus $B$ for $\alpha = 1$

Figure 4 accounts for the dependence of $\alpha_c$ and $R_c$ on $B$. The already discussed limit $B \to 0$ can be evinced as one infers a gradual decrease to zero of $\alpha_c$ and an asymptotic approach to $R_c = 12$. Just the same happens for the limit $B \to \infty$ embodying the case where the upper boundary is perfectly isothermal. In this case, we have

$$\alpha_c = 2.32621, \qquad R_c = 27.0976. \tag{27}$$

The results for the limiting cases $B \to 0$ and $B \to \infty$ are in perfect agreement with what is reported in Nield and Bejan [2].

An alternative approach is the analytical solution of Eqs. (26), with $\eta = 0$. This task is feasible as the ordinary differential equations (26a) and (26b) have constant coefficients. The analytical solution procedure yields nonzero $(f, h)$ provided that the dispersion relation

$$\frac{\sinh\zeta_1}{\zeta_1}\left(\frac{\alpha^2\sin\zeta_2}{\zeta_2} + B\cos\zeta_2\right) + \cosh\zeta_1\left(\frac{B\sin\zeta_2}{\zeta_2} + \cos\zeta_2\right) - 1 = 0, \tag{28}$$

is satisfied, where

$$\zeta_1 = \sqrt{\alpha\left(\sqrt{R} + \alpha\right)}, \qquad \zeta_2 = \sqrt{\alpha\left(\sqrt{R} - \alpha\right)}. \tag{29}$$

Equation (29) provides an implicit expression of the neutral stability condition, where $R$ is evaluated versus $\alpha$ for prescribed $B$. Table 1 reports the neutral stability values of $R$ with $\alpha = 1$ for different Biot numbers. The results reported in this table were obtained by both approaches, shooting method and analytical dispersion relation, yielding a perfect agreement within all the 15 significant figures.

An aspect regarding the behaviour for small Biot numbers is the huge sensitivity to $B$ of the neutral stability threshold when $\alpha$ is very close to zero, *i.e.*, in the limit where normal modes have infinite

wavelength. This feature emerges by inspecting Fig. 2. In fact, this figure suggests that, for small $\alpha$, even a minimal uncertainty on the value of $B$ may result into a practically unpredictable neutral stability value of $R$. This feature can be demonstrated by means of Eqs. (28) and (29) on keeping the first dominant terms in a series expansion with respect to $\alpha$ around $\alpha = 0$, namely

$$R = \frac{60B}{\alpha^2\,(2B+5)} - \frac{40}{2B+5} + 20. \tag{30}$$

When $B = 0$, Eq. (30) yields $R = 12$, which is the expected result already pointed out above. When $B > 0$, in the regime $\alpha^2 \ll 1$, Eq. (30) can be approximated as

$$R = \frac{60B}{\alpha^2\,(2B+5)}. \tag{31}$$

The sensitivity to $B$ of the neutral stability value, $R$, when $\alpha$ is very close to zero is estimated through the derivative,

$$\frac{\partial R}{\partial B} = \frac{300}{\alpha^2(2B+5)^2}. \tag{32}$$

This expression of $\partial R/\partial B$ shows that, when $\alpha$ is very small, a minimum uncertainty in the value of $B$ results into a dramatic uncertainty in the determination of $R$. This is a specially strong effect when $B$ is small. The physical meaning is that the response of the basic flow to normal modes with very long wavelengths is extremely different if we assume $B = 0$, or a positive but very small $B$. A similar severe sensitivity to a parameter was pointed out by Sphaier et al. [32] relative to the effect of a small inclination angle to the horizontal on the onset of convective instability in a uniformly heated porous channel. Such sensitivity issues are to be taken into account in the design of an experiment regarding the onset of instability.

### *4.2. Response to wavepacket perturbations or the onset of absolute instability*

The starting point for the analysis of the onset of absolute instability are Eqs. (17), complemented by the two conditions expressed by Eqs. (21) and (22). Dealing numerically with such an analysis suggests the definition,

$$\tilde{f} = \frac{\partial f}{\partial k}, \qquad \tilde{h} = \frac{\partial h}{\partial k}. \tag{33}$$

allowing, based on Eqs. (17), the definition of the extended eigenvalue problem,

$$f'' - \left(k^2 + s\right)(f + R\,h) = 0, \tag{34a}$$

$$h'' - \lambda(k)\,h - \left(k^2 + s + ikP\right)h - f = 0, \tag{34b}$$

$$\tilde{f}'' - \left(k^2 + s\right)\left(\tilde{f} + R\,\tilde{h}\right) - 2k\,(f + R\,h) = 0, \tag{34c}$$

$$\tilde{h}'' - \lambda(k)\,\tilde{h} - \left(k^2 + s + ikP\right)\tilde{h} - \tilde{f} - (2k + iP)\,h = 0, \tag{34d}$$

$$z = 0 \;:\qquad f = 0, \quad h' = 0, \quad \tilde{f} = 0, \quad \tilde{h}' = 0, \tag{34e}$$

$$z = 1 \;:\qquad f = 0, \quad h' + Bh = 0, \quad \tilde{f} = 0, \quad \tilde{h}' + B\tilde{h} = 0, \tag{34f}$$

as described in detail elsewhere [14]. We mention that, on writing Eq. (34d), we implicitly employed Eq. (21). We also assumed $B$, $P$ and $R$ as input parameters and, hence, independent of $k$. In Eqs. (34), we employed the notation

$$s = \frac{n^2\pi^2}{A^2}, \tag{35}$$

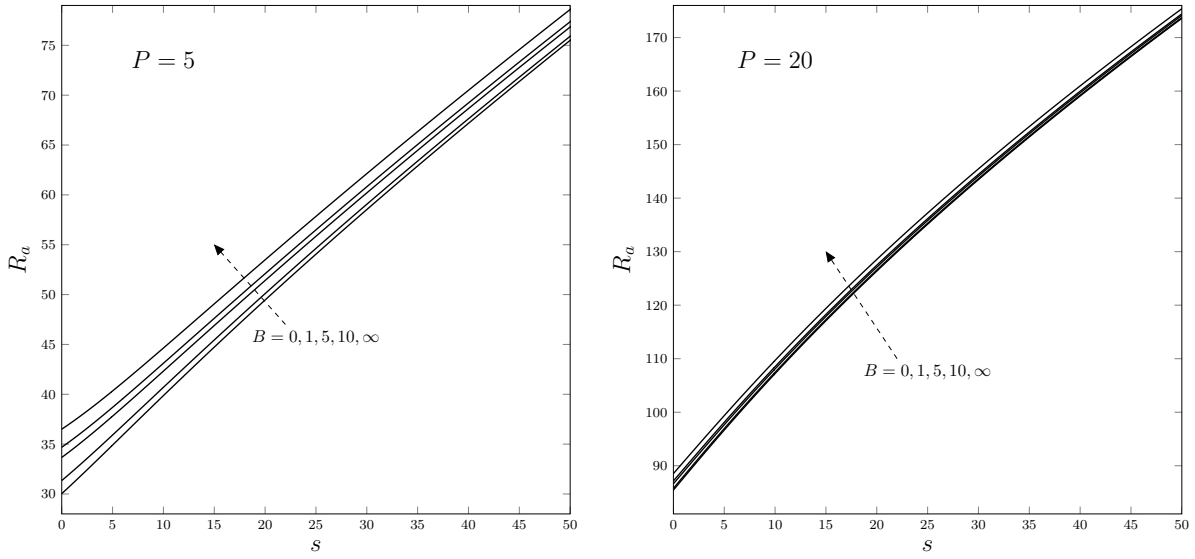


Figure 5: Onset of absolute instability: plots of $R_a$ versus $s$ for different $B$ with either $P = 5$ or $P = 20$

so that the special case $s = 0$ identifies either the $n = 0$ modes or the limit $A \to \infty$ with $n \neq 0$. Both these cases involve $y$ independent (and, hence, two–dimensional) perturbations as one can infer from Eq. (10). Every positive value of $s$ corresponds to infinite possible pairs $(n, A)$ with $n \neq 0$. All these pairs identify three–dimensional perturbation modes.

The solution of the eigenvalue problem (34) allows us to evaluate the four unknowns

$$\mathfrak{Re}(k),\ \mathfrak{Im}(k),\ \mathfrak{Im}(\lambda),\ R, \tag{36}$$

for every given set of input data,

$$s,\ B,\ P, \tag{37}$$

and $\mathfrak{Re}(\lambda) = 0$. The latter statement is a consequence of Eq. (22) given that the values of $\mathfrak{Re}(k)$ and $\mathfrak{Im}(k)$ included in Eq. (36) are those identifying the pertinent saddle point for the transition to absolute instability. Likewise, the value of $R$ listed in Eq. (36) is that marking this transition. Hereafter, this threshold value of $R$ will be denoted as $R_a$, where "$a$" stands for absolute instability.

The solution of the eigenvalue problem (34) can be approached numerically, much in the same way as we did for the corresponding convective instability eigenvalue problem (26). Here, the complexity is enhanced due to the doubled order of the system of differential equations. We set up the shooting method by first formulating a consistent initial value problem,

$$f'' - \left(k^2 + s\right)(f + R\,h) = 0, \tag{38a}$$

$$h'' - \lambda(k)\,h - \left(k^2 + s + ikP\right)h - f = 0, \tag{38b}$$

$$\tilde{f}'' - \left(k^2 + s\right)\left(\tilde{f} + R\,\tilde{h}\right) - 2k\,(f + R\,h) = 0, \tag{38c}$$

$$\tilde{h}'' - \lambda(k)\,\tilde{h} - \left(k^2 + s + ikP\right)\tilde{h} - \tilde{f} - (2k + iP)\,h = 0, \tag{38d}$$

$$\begin{aligned} &f(0) = 0, \quad f'(0) = 1, \quad h(0) = r_1 + i\,r_2, \quad h'(0) = 0, \\ &\tilde{f}(0) = 0, \quad \tilde{f}'(0) = 0, \quad \tilde{h}(0) = \tilde{r}_1 + i\,\tilde{r}_2, \quad \tilde{h}'(0) = 0. \end{aligned} \tag{38e}$$

Here, we prescribe $f'(0) = 1$ as a scale–fixing condition for the eigenfunctions, $(f, h, \tilde{f}, \tilde{h})$. Then, the homologous condition $\tilde{f}'(0) = 0$ comes out as a natural consequence of Eq. (33). Four extra unknowns

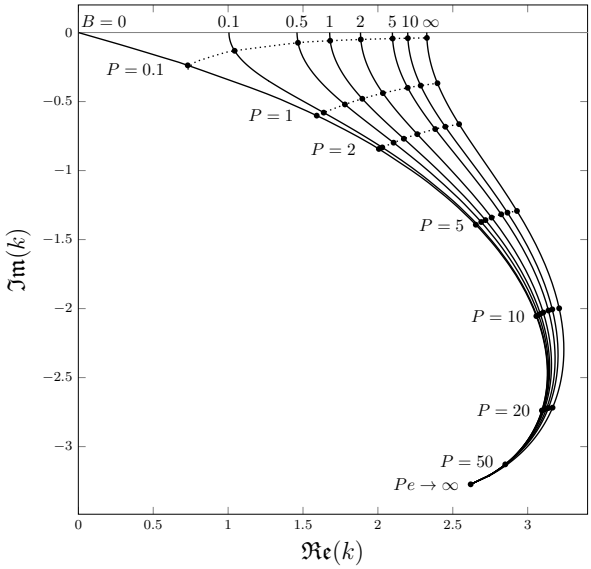


Figure 6: Onset of absolute instability: position of the saddle points $k$ in the complex plane for given Biot numbers and variable Péclet number. The dots connected by dotted lines show up the positions at some special values of $P$

have been introduced, $r_1$, $r_2$, $\tilde{r_1}$ and $\tilde{r_2}$. These four unknowns, together with those listed in Eq. (36) lead to a total of eight real unknowns. Such eight unknowns can be evaluated by satisfying the end conditions,

$$f(1) = 0, \quad h'(1) + Bh(1) = 0, \quad \tilde{f}(1) = 0, \quad \tilde{h}'(1) + B\tilde{h}(1) = 0. \tag{39}$$

In fact, the four complex equations (39) correspond to eight real equations, through their real and imaginary parts. Thus, they are enough to evaluate the eight unknown parameters, $r_1$, $r_2$, $\tilde{r_1}$, $\tilde{r_2}$, $\mathfrak{Re}(k)$, $\mathfrak{Im}(k)$, $\mathfrak{Im}(\lambda)$ and $R$.

The evaluated thresholds to absolute instability are represented in Fig. 5 with reference to a pair of different Péclet numbers, $P = 5$ and $P = 20$, and to different Biot numbers. The value of $R_a$ is evidently an increasing function of $s$ for every Péclet number and Biot number considered in this figure. This trend suggests that the most unstable perturbations triggering the transition to absolute instability are two–dimensional ($s = 0$), as they provide the lowest value of $R_a$. On the basis of this finding, we are justified in focussing our forthcoming discussion of results on the two–dimensional analysis of absolute instability, where only the case $s = 0$ is entailed. There is another aspect that will be further explored later on. As the Péclet number increases, the influence of the Biot number on the threshold value $R_a$ becomes very weak. As it is shown in Fig. 5, with $P = 20$, the curves corresponding to very different Biot numbers are hardly discernible.

## 5. Discussion of the results

An important symmetry of the eigenvalue problem (34) can be found for every fixed input data $(s, B, P)$, with $\mathfrak{Re}(\lambda) = 0$. If

$$\mathfrak{Re}(k), \ \mathfrak{Im}(k), \ \mathfrak{Im}(\lambda), \ R \tag{40}$$

are eigenvalues for Eqs. (34) corresponding to the eigenfunctions $(f, h, \tilde{f}, \tilde{h})$, then also

$$-\mathfrak{Re}(k), \ \mathfrak{Im}(k), \ -\mathfrak{Im}(\lambda), \ R \tag{41}$$

are allowed eigenvalues, which correspond to the eigenfunctions $(f, h, -\tilde{f}, -\tilde{h})$. With this property in mind, it is not restrictive to assume $\mathfrak{Re}(k) \geqslant 0$ while searching the pertinent saddle points for the

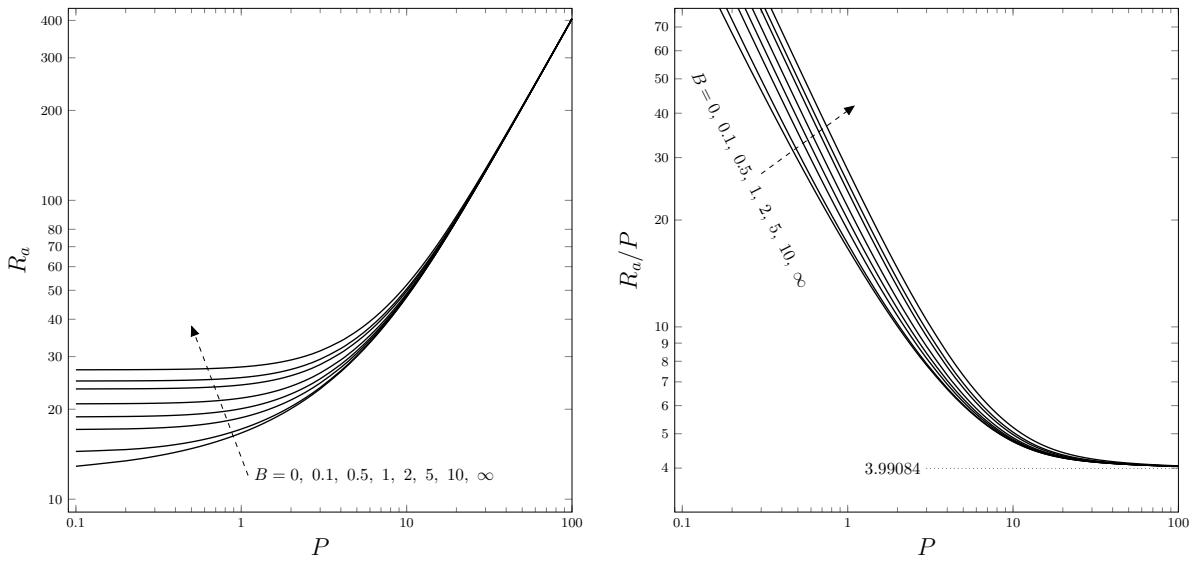


Figure 7: Onset of absolute instability with $s = 0$: plots of $R_a$ versus $P$ and $R_a/P$ versus $P$ for different values of $B$

transition to absolute instability in the complex plane $k \in \mathbb{C}$. The position of these saddle points at different Biot numbers and Péclet numbers is displayed in Fig. 6. This figure allows one to trace the migration of the saddle point $k$ associated with the transition to absolute instability from the real axis, $\mathfrak{Im}(k) = 0$, when $P = 0$, to positions with $\mathfrak{Im}(k) < 0$, at positive values of $P$. That the saddle points with $P = 0$ are located on the real $k$ axis is a consequence of the identity $R_c = R_a$, in the absence of a net horizontal troughflow. In other words, when $P = 0$, the saddle point $k$ is real and coincides with $k_c$. It is zero when $B = 0$ and gradually increases reaching asymptotically the value 2.32621 in the limit $B \to \infty$. As $P > 0$, the saddle points for different Biot numbers are complex and gradually depart from the axis $\mathfrak{Im}(k) = 0$. An important property reflected by Fig. 6 is that the dependence on the Biot number becomes very weak when $P$ is large. Moreover, Fig. 6 shows that, in the limit $P \to \infty$, there exists a limiting position of the saddle point which is independent of the Biot number. This feature can be proved rigorously starting from Eqs. (17). We introduce the scaling

$$R = \tau\, P, \qquad \lambda = \Lambda\, P, \qquad f = F\, P, \tag{42}$$

so that, when $P \gg 1$, we attain the asymptotic eigenvalue problem

$$F'' + k^2 \left( \frac{\tau}{\Lambda + i\, k} - 1 \right) F = 0, \tag{43a}$$

$$z = 0, 1 \ : \qquad F = 0, \tag{43b}$$

having in mind that our clue is the analysis of two–dimensional perturbations, namely $n = 0$ or $s = 0$. We note that, due to the reduced differential order of Eqs. (43) with respect to Eqs. (17), the boundary conditions on the eigenfunction $h$ cannot be adjusted anymore. Equations (43) can be solved, up to an arbitrary multiplicative constant, with

$$F(z) = \sin(\pi \ell z), \qquad \text{with} \quad \ell = 1, 2, 3, \ \dots \ , \tag{44}$$

provided that

$$k^2 \left( \frac{\tau}{\Lambda + i\, k} - 1 \right) - \pi^2 \ell^2 = 0. \tag{45}$$

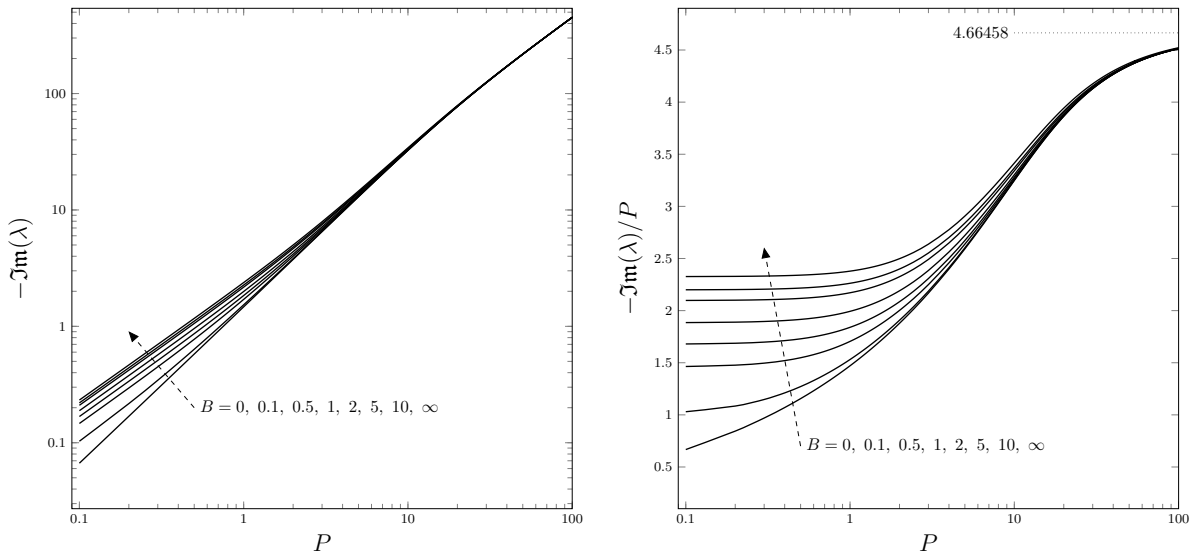


Figure 8: Onset of absolute instability with $s = 0$: plots of $-\mathfrak{Im}(\lambda)$ versus $P$ and $-\mathfrak{Im}(\lambda)/P$ versus $P$ for different values of $B$

One may obtain $\Lambda(k)$ from Eq. (45) and, then, evaluate its derivative $\Lambda'(k)$. By prescribing the saddle–point condition, $\Lambda'(k) = 0$, together with the threshold condition for absolute instability, $\mathfrak{Re}(\Lambda(k)) = 0$, one finally attains the explicit expression for the saddle point $k$ in the complex plane,

$$k = \frac{\pi\ell}{4}\sqrt{\sqrt{17}+7} - \frac{i\pi\ell}{4}\sqrt{3\sqrt{17}+5}, \tag{46}$$

as well as for $\tau$ and $\mathfrak{Im}(\Lambda)$,

$$\tau = \frac{\pi\ell}{16}\left(9-\sqrt{17}\right)\sqrt{3\sqrt{17}+5}, \qquad \mathfrak{Im}(\Lambda) = -\frac{\pi\ell}{8}\sqrt{17\sqrt{17}+71}. \tag{47}$$

As we are interested in the least threshold value $\tau$ we have to choose $\ell = 1$ in Eqs. (46) and (47), so that

$$k \approx 2.61941 - 3.27327\,i, \qquad \tau \approx 3.99084, \qquad \mathfrak{Im}(\Lambda) \approx -4.66458. \tag{48}$$

Finally, by employing Eq. (42), we find the asymptotic solution for $P \gg 1$,

$$k \approx 2.61941 - 3.27327\,i, \qquad R_a \approx 3.99084\,P, \qquad \mathfrak{Im}(\lambda) \approx -4.66458\,P. \tag{49}$$

The complex $k$ reported in Eq. (49) is graphically represented in Fig. 6 as the limit $P \to \infty$. The second equation (49) also highlights mathematically an important physical characteristic of the present problem. The onset of absolute instability entails the parametric conditions beyond which downstream propagating wavepackets will start to propagate upstream as well. In order to achieve it, thermal energy must be provided to these wavepakets, through $R$, for them to overcome the basic flow advecting them downstream. Hence, when advection becomes stronger, which occurs by increasing $P$, the minimum amount of thermal energy required for absolute instability, $R_a$, must increase as well. Equation (49) proves this is true for the present problem and, additionally, it shows that $R_a$ is proportional to $P$.

Another feature of the large Péclet number regime inferred from Eq. (40) is the linearly increasing trend of $R_a$ with $P$, together with the linearly decreasing trend of $\mathfrak{Im}(\lambda)$. Such trends are in fact retrieved by getting the numerical values of $R_a$ and $\mathfrak{Im}(\lambda)$ for given values of $P$ and $B$. An illustration of this feature is found in Fig. 7 where the threshold Darcy–Rayleigh number for the onset of absolute instability, $R_a$, is plotted versus $P$ spanning the whole range of positive values for the Biot number, $B$. This figure

| | $P=0.5$ | | $P=1$ | | $P=5$ | | $P=10$ | |
|---|---|---|---|---|---|---|---|---|
| $B$ | $R_c$ | $R_a$ | $R_c$ | $R_a$ | $R_c$ | $R_a$ | $R_c$ | $R_a$ |
| 0 | 12 | 14.7667 | 12 | 16.6548 | 12 | 30.0307 | 12 | 47.4877 |
| 0.01 | 12.7456 | 14.8523 | 12.7456 | 16.7088 | 12.7456 | 30.0471 | 12.7456 | 47.4962 |
| 0.1 | 14.3607 | 15.5416 | 14.3607 | 17.1658 | 14.3607 | 30.1916 | 14.3607 | 47.5708 |
| 1 | 18.8505 | 19.2116 | 18.8505 | 20.0871 | 18.8505 | 31.3470 | 18.8505 | 48.2053 |
| 10 | 24.8549 | 25.0306 | 24.8549 | 25.5236 | 24.8549 | 34.6867 | 24.8549 | 50.4936 |
| 100 | 26.8203 | 26.9786 | 26.8203 | 27.4285 | 26.8203 | 36.2578 | 26.8203 | 51.8681 |
| $\infty$ | 27.0976 | 27.2542 | 27.0976 | 27.6998 | 27.0976 | 36.4994 | 27.0976 | 52.1000 |

Table 2: Critical value $R_c$ and absolute instability threshold $R_a$ obtained for different $B$ and $P$

clearly shows that $B$ becomes effectively irrelevant when $P$ becomes very large, say larger than 20. This, then, is the transition to a regime where $R_a$ varies linearly with $P$ as predicted in Eq. (49). Figure 7 allows one to compare the threshold $R_a$ with the critical value $R_c$, which describes the transition to absolute instability, graphically identified as the limit of $R_a$ when $P \to 0$. Indeed, the gap $R_a - R_c$ undergoes a dramatic increase with $P$. This means, physically, that a large flow rate prevents the instability to localised perturbations, *i.e.* wavepackets, while it does not affect in any way the growth of uniformly spread perturbations such as plane waves, *i.e.* Fourier normal modes with a given wavenumber. Numerical data for the threshold to convective instability, $R_c$, and for the threshold to absolute instability, $R_a$, are reported in Table 2 for different values of $B$ and $P$.

Figure 8 adds further information on the transition to absolute instability through the plots of $-\mathfrak{Im}(\lambda)$ and $-\mathfrak{Im}(\lambda)/P$ versus $P$ for different Biot numbers. The physical meaning of $-\mathfrak{Im}(\lambda)$ is, up to the multiplicative constant $\xi$, that of an angular frequency in either cases of pure Fourier normal modes and of wavepackets. In the former case, the angular frequency depends on the wavenumber of the normal mode. In the case of wavepackets, the physical meaning of angular frequency emerges at large times as a consequence of the steepest–descent approximation [15]. Figure 8 discloses the existence of asymptotic constant values of the ratio $-\mathfrak{Im}(\lambda)/P$ when either $P \to 0$ or $P \to \infty$. While the latter is independent of $B$ as a consequence of Eq. (49), the former depends on $B$ due to the coincidence of the thresholds to convective and to absolute instability. In particular, this implies that for $P \to 0$ we have $R_a = R_c$ with the saddle point, $k$, real and equal to $k_c$. In fact, as we pointed out in Section 4.1, the principle of exchange of stabilities in the co-moving reference frame yields, at critical conditions,

$$-\mathfrak{Im}(\lambda) = k_c P, \tag{50}$$

as implied by Eq. (24). This means that the asymptotic value of $-\mathfrak{Im}(\lambda)/P$ when $P \to 0$ is $k_c$, namely a quantity dependent on $B$ as displayed in Fig. 4. Figure 8 strengthens our conclusion that the dependence on the Biot number is significant only for sufficiently small $P$, while at larger $P$ the imaginary part of $\lambda$ at the saddle point becomes almost independent of $B$ or, in other words, it is almost independent of the temperature boundary conditions.

All parametric conditions for the wavepacket instability were calculated based on the saddle point location provided by Eq. (21). This is, however, a necessary but not sufficient condition for the onset of absolute instability. The use of the steepest–descent approximation in order to assess the large–time behaviour of wavepacket perturbations of the basic flow requires the holomorphy condition to be satisfied [15]. In other words, there must exist a continuous mapping such that the real axis, $\mathfrak{Im}(k) = 0$, is deformed into a path crossing the saddle point along a curve which is, locally, of steepest descent [15, 27, 28]. This geometrical deformation needs to be done without crossing any singularity of $\lambda(k)$. In order to check that this is the case one may employ diagrams such as those reported in Fig. 9, where the isolines of $\mathfrak{Re}(\lambda)$ are drawn for $P = 1$ and different Biot numbers. The saddle point is visualized as the intersection of the

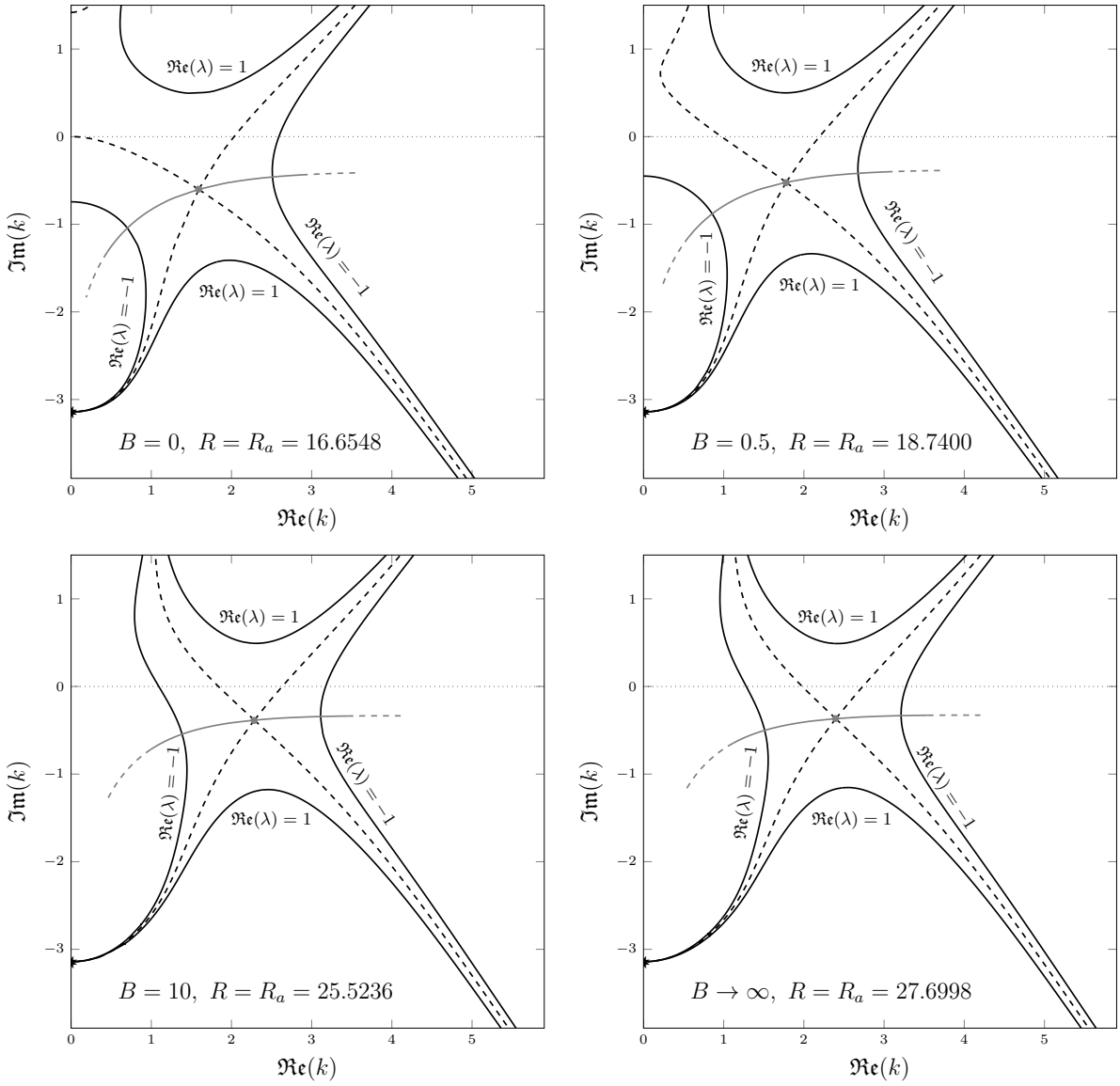


Figure 9: Maps of the isolines of $\mathfrak{Re}(\lambda)$ (black solid lines) for $P = 1$ and $R = R_a$ with different values of $B$. The dashed black lines are for $\mathfrak{Re}(\lambda) = 0$. The grey dots are the saddle points, while the grey lines are the lines of steepest descent. The black asterisk denotes the singularity occurring at $k = -i\pi$

isolines with $\mathfrak{Re}(\lambda) = 0$ and the path of steepest descent is shown as well. In these diagrams, a singularity is an attraction point for the isolines with all possible values of $\mathfrak{Re}(\lambda)$. In fact, in Fig. 9, a singularity is displayed in every frame for $k = -i\pi$. That such a point yields a singularity of $\lambda(k)$ is evident for the limiting case of a very large Péclet number. In fact, in this case, Eq. (45) holds. If one solves this equation for $\Lambda(k)$ with $\ell = 1$, one immediately concludes that $\Lambda(k)$ is singular when $\pi^2 + k^2 = 0$. For all the Biot numbers considered in Fig. 9, the holomorphy requirement is satisfied as one can deform the real $k$ axis into a path crossing the saddle point along a line which is locally of steepest descent, without interlacing the singularity $k = -i\pi$. In principle, this check should be iterated for all possible Péclet numbers. In this paper, for the sake of brevity, we reported only the case $P = 1$ as one where the distinction between diverse Biot numbers is evident. As $P$ increases, the dependence on $B$ becomes weaker and weaker until the asymptotic regime of very large $P$ is attained. In this regime, described by Eqs. (42)–(49), the holomorphy condition is satisfied as illustrated in Fig. 8.13 of the book by Barletta [15].

Finally, it is important to note that the problem defined by Eqs. (34) can be restated in alternative ways. One such way is to reduce Eqs. (34a)–(34d) to

$$h'''' - \left[\,\lambda(k) + 2\left(k^2+s\right) + i\,k\,P\,\right] h'' + \left(k^2+s\right)\left[\,\lambda(k) + k^2 + s + i\,k\,P - R\,\right] h = 0, \tag{51a}$$

$$\begin{aligned}\tilde{h}'''' - \left[\,\lambda(k) + 2\left(k^2+s\right) + i\,k\,P\,\right] \tilde{h}'' + \left(k^2+s\right)\left[\,\lambda(k) + k^2 + s + i\,k\,P - R\,\right] \tilde{h} \\ = \left[\,h'' - \left(k^2+s\right) h\,\right] \lambda'(k) - 2\,k\,h\,\lambda(k) + (4\,k + i\,P)\,h'' \\ - \left(4\,k^3 + 3\,i\,k^2\,P - 2\,k\,R + 4\,k\,s + i\,P\,s\right) h,\end{aligned} \tag{51b}$$

$$\begin{aligned} z = 0 \;:\quad & h' = 0, \quad h'' - \left[\,\lambda(k) + k^2 + s + i\,k\,P\,\right] h = 0, \\ & \tilde{h}' = 0, \quad \tilde{h}'' - \left[\,\lambda(k) + k^2 + s + i\,k\,P\,\right] \tilde{h} = \left[\,2\,k + i\,P\,\lambda'(k)\,\right] h, \end{aligned} \tag{51c}$$

$$\begin{aligned} z = 1 \;:\quad & h' + Bh = 0, \quad h'' - \left[\,\lambda(k) + k^2 + s + i\,k\,P\,\right] h = 0, \\ & \tilde{h}' + B\tilde{h} = 0, \quad \tilde{h}'' - \left[\,\lambda(k) + k^2 + s + i\,k\,P\,\right] \tilde{h} = \left[\,2\,k + i\,P\,\lambda'(k)\,\right] h, \end{aligned} \tag{51d}$$

achieved by eliminating $f(z)$ and $\tilde{f}(z)$. Equations (51) are equivalent to Eqs. (34a)–(34d), producing the same results. There is yet another restatement of this problem that is interesting to mention because of its relation to Eq. (21). Fredholm alternative theorem [33], when applied to linear elliptic boundary value problems, states that nontrivial solutions of the inhomogeneous Eq. (51b) can only exist when the inhomogeneous source term of Eq. (51b) is orthogonal to the adjoint solution of the homogeneous Eq. (51a). However, Fredholm alternative theorem requires that the boundary conditions for Eq. (51b) be homogeneous, which is not the case of the conditions for $\tilde{h}$ given by Eqs. (51c) and (51d) as they contain also $h$. Hence, Fredholm alternative theorem cannot be applied to Eq. (51b). In order to encompass this difficulty, these boundary conditions must be homogenized. To do so, one needs to apply the transformation

$$\tilde{h}(z) - \left[2\,k + i\,P\,\lambda'(k)\right] \mathcal{F}(z)\,h(z) \to \tilde{h}(z), \quad \text{where} \quad \mathcal{F}(z) = \frac{z^2\,(z-1)^2}{2}. \tag{52}$$

We now denote by $\mathcal{H}(z)$ the adjoint of $h(z)$. Then, Fredholm alternative theorem, also known as solvability condition, can be used to generate the following expression

$$\begin{aligned}\lambda'(k) = -\Bigg\{ & \left[4\,k\,s - 2\,k\,R + 3\,i\,k^2\,P + 4\,k^3 + i\,P\,s + 2\,k\,\lambda(k)\right] \int_0^1 h\,\bar{\mathcal{H}}\,dz \\ & + \left(k^2+s\right)\left[\,\lambda(k) + k^2 + s + i\,k\,P - R\,\right](2\,k + i\,P) \int_0^1 \mathcal{F}\,h\,\bar{\mathcal{H}}\,dz \\ & - (4\,k + i\,P) \int_0^1 h''\,\bar{\mathcal{H}}\,dz - \left[\lambda(k) + 2\left(k^2+s\right) + i\,k\,P\right](2\,k + i\,P) \int_0^1 (\mathcal{F}\,h)''\;\bar{\mathcal{H}}\,dz \\ & + (2\,k + i\,P) \int_0^1 (\mathcal{F}\,h)''''\;\bar{\mathcal{H}}\,dz \Bigg\} \Bigg/ \Bigg\{ \left(k^2+s\right) \Bigg\{ \int_0^1 h\,\bar{\mathcal{H}}\,dz \\ & + \left[\,\lambda(k) + k^2 + s + i\,k\,P - R\,\right] \int_0^1 \mathcal{F}\,h\,\bar{\mathcal{H}}\,dz \Bigg\} - \int_0^1 h''\,\bar{\mathcal{H}}\,dz \\ & - \left[\,\lambda(k) + 2\left(k^2+s\right) + i\,k\,P\,\right] \int_0^1 (\mathcal{F}\,h)''\;\bar{\mathcal{H}}\,dz + \int_0^1 (\mathcal{F}\,h)''''\;\bar{\mathcal{H}}\,dz \Bigg\}, \end{aligned} \tag{53}$$

where the overbar means complex conjugation. Hence, solving Eq. (51a) and setting, through Eq. (53), $\lambda'(k)$ equal to zero is equivalent to solving Eq. (51a) with either Eq. (51b) or Eq. (53), since it produces the same results. A detailed discussion about the derivation of adjoint equations, group velocity expressions as well as alternative ways to find saddle points can be found in Alves et al. [14]. It is important to mention, however, that all governing equations in the examples provided in this reference have homogeneous boundary conditions. Hence, the homogenization procedure defined by Eq. (52) is a novel contribution to this subject. In fact, Eq. (53) is employed to calculate $\lambda'(k)$ for several saddle points provided in Table 2. In all cases, it yields zero within a user prescribed tolerance, thus validating this equation.

## 6. Conclusions

The transition from stability to convective instability and the transition from convective instability to absolute instability have been studied for small–amplitude, *i.e.* linear, perturbations superposed to a basic uniform flow in a horizontal porous channel saturated by a fluid.

The buoyancy–driven instability is triggered by a prescribed heat flux at the lower boundary, while the upper boundary is cooled by heat transfer to the external environment. The latter mechanism is governed by the Biot number, $B$, while the dimensionless flow rate is given by the Péclet number, $P$. The dimensionless number proportional to the wall heat flux supplied from below is the Darcy–Rayleigh number, $R$. This number is the order parameter for the transition to instability, either convective or absolute. The channel is confined laterally by thermally insulated sidewalls. These conditions serve to formulate the three–dimensional instability analysis.

The convective instability happens when Fourier normal modes of perturbation, with a given wavenumber $k$, exponentially grow in time. This condition may arise when $R$ exceeds its critical value, $R_c$. The absolute instability happens when the amplitude of wavepacket perturbations, expressed as a Fourier integral along the streamwise direction, tends to infinity as time tends to infinity. The two concepts coincide when $P = 0$, while absolute instability arises with supercritical values of $R$ when $P \neq 0$.

The thresholds for the convective instability and for the absolute instability have been determined numerically, by a shooting–method algorithm for differential eigenvalue problems. Furthermore, an analytical dispersion relation has been obtained for the convective instability. The most interesting aspects of the study carried out in this paper are the following:

- The convective instability versus large wavelength perturbations is strongly sensitive to the value of $B$, especially when $B$ is small. Thus, a weak departure from the perfect isoflux condition at the upper boundary, expressed as $B = 0$, may result into an effectively unpredictable value of $R$ for neutral stability.

- The transition to absolute instability takes place with two–dimensional perturbations. The steepest–descent approximation of perturbation wavepackets provides the mathematical condition for establishing the large–time growth or damping of the wavepacket. The numerical implementation of this condition yields an eigenvalue problem which has been solved numerically yielding, for every prescribed pair $(P, B)$, the threshold value $R = R_a$ for the transition to absolute instability.

- Numerical values of $R_a$ were obtained leading us to the conclusion that, for every $B$, $R_a$ is a monotonic increasing function of $P$ and, for every $P$, $R_a$ is a monotonic increasing function of $B$. Thus, the condition of isothermal upper boundary, $B \to \infty$, yields the most stable setup for the flow.

- An asymptotic condition for large Péclet numbers has been identified such that $R_a$ changes linearly with $P$ and displays a negligible dependence on $B$.

There are several directions for future developments of this research. Most of them head to the nonlinear domain where the limits of the present linear analysis can be quantified. An important information to be gathered from a nonlinear analysis regards the mechanism of nonlinear saturation where the initially exponential time growth of unstable perturbations, predicted by the linear analysis, may turn into an asymptotically stationary condition involving buoyancy–induced convection patterns with a finite increase of heat transfer rates. Another interesting aspect could emerge by revisiting the absolute instability concept in the light of the nonlinear energy method [31, 34, 35]. This approach may shed a new light on

the role of nonlinearity in the wavepacket dynamics and on the estimation of the large–time growth rates of localised perturbations.

### Declaration of competing interest

The authors declared that there is no conflict of interest.


### Acknowledgements

This study was financed in part by the Coordenação de Aperfeiçoamento de Pessoal de Nível Superior - Brazil (CAPES) - Grant n° 88881.174085/2018-01. Financial support was also provided by Ministero dell'Istruzione, dell'Università e della Ricerca (Italy) – Grant n° PRIN2017F7KZWS.


### References


[1] M. Prats, The effect of horizontal fluid flow on thermally induced convection currents in porous mediums, Journal of Geophysical Research 71 (1966) 4835–4838.

[2] D. A. Nield, A. Bejan, Convection in Porous Media, 5th Edition, Springer, New York, 2017.

[3] R. J. Briggs, Electron-Stream Interaction with Plasmas, MIT Press, Cambridge, MA, 1964.

[4] A. Bers, Space-time evolution of plasma instabilities - absolute and convective, in: A. A. Galeev, R. N. Sudan (Eds.), Basic Plasma Physics, Vol. 1, North-Holland, 1983, pp. 451–517.

[5] E. M. Lifshitz, L. P. Pitaevskii, Physical Kinetics, Pergamon Press, Oxford, 1981.

[6] L. D. Landau, E. M. Lifshitz, Fluid Mechanics, Pergamon Press, Oxford, 1987.

[7] P. G. Drazin, W. H. Reid, Hydrodynamic Stability, 2nd Edition, Cambridge University Press, New York, NY, 2004.

[8] P. Huerre, P. A. Monkewitz, Absolute and convective instabilities in free shear layers, Journal of Fluid Mechanics 159 (1985) 151–168.

[9] P. Huerre, P. A. Monkewitz, Local and global instabilities in spatially developing flows, Annual Review of Fluid Mechanics 22 (1990) 473–537.

[10] P. Carrière, P. A. Monkewitz, Convective versus absolute instability in mixed Rayleigh-Bénard-Poiseuille convection, Journal of Fluid Mechanics 384 (1999) 243–262.

[11] P. J. Schmid, D. S. Henningson, Stability and Transition in Shear Flows, Springer, New York, 2012.

[12] M. P. Juniper, A. Hanifi, V. Theofilis, Modal stability theory, Applied Mechanics Reviews 66 (2014) 024804.

[13] S. A. Suslov, Numerical aspects of searching convective/absolute instability transition, Journal of Computational Physics 212 (2006) 188–217.

[14] L. S. de B. Alves, S. C. Hirata, M. Schuabb, A. Barletta, Identifying linear absolute instabilities from differential eigenvalue problems using sensitivity analysis, Journal of Fluid Mechanics 870 (2019) 941–969.

[15] A. Barletta, Routes to Absolute Instability in Porous Media, Springer, New York, 2019.

[16] C. W. Horton, F. T. Rogers, Convection currents in a porous medium, Journal of Applied Physics 16 (1945) 367–370.

[17] E. R. Lapwood, Convection of a fluid in a porous medium, Proceedings of the Cambridge Philosophical Society 44 (1948) 508–521.

[18] A. Delache, M. N. Ouarzazi, M. Combarnous, Spatio–temporal stability analysis of mixed convection flows in porous media heated from below: Comparison with experiments, International Journal of Heat and Mass Transfer 50 (2007) 1485–1499.

[19] L. Brevdo, M. S. Ruderman, On the convection in a porous medium with inclined temperature gradient and vertical throughflow. Part I. normal modes, Transport in Porous Media 80 (2009) 137–151.

[20] L. Brevdo, M. S. Ruderman, On the convection in a porous medium with inclined temperature gradient and vertical throughflow. Part II. absolute and convective instabilities, and spatially amplifying waves, Transport in Porous Media 80 (2009) 153–172.

[21] L. Brevdo, Three–dimensional absolute and convective instabilities at the onset of convection in a porous medium with inclined temperature gradient and vertical throughflow, Journal of Fluid Mechanics 641 (2009) 475–487.

[22] S. C. Hirata, M. N. Ouarzazi, Three-dimensional absolute and convective instabilities in mixed convection of a viscoelastic fluid through a porous medium, Physics Letters A 374 (2010) 2661–2666.

[23] L. S. de B. Alves, A. Barletta, Convective to absolute instability transition in the Prats flow of a power-law fluid, International Journal of Thermal Sciences 94 (2015) 270–282.

[24] A. Barletta, L. S. de B. Alves, Absolute instability: A toy model and an application to the Rayleigh–Bénard problem with horizontal flow in porous media, International Journal of Heat and Mass Transfer 104 (2017) 438–455.

[25] A. Barletta, M. Celli, Convective to absolute instability transition in a horizontal porous channel with open upper boundary, Fluids 2 (2017) 33.

[26] A. C. King, J. Billingham, S. R. Otto, Differential Equations: Linear, Nonlinear, Ordinary, Partial, Cambridge University Press, 2003.

[27] C. M. Bender, S. A. Orszag, Advanced Mathematical Methods for Scientists and Engineers I, Springer, New York, 1999.

[28] M. J. Ablowitz, A. S. Fokas, Complex Variables: Introduction and Applications, Cambridge University Press, Cambridge, 2003.

[29] A. Pellew, R. V. Southwell, On maintained convective motion in a fluid heated from below, Proceedings of the Royal Society of London. Series A. Mathematical and Physical Sciences 176 (1940) 312–343.

[30] L. S. de B. Alves, A. Barletta, Convective instability of the Darcy–Bénard problem with through flow in a porous layer saturated by a power–law fluid, International Journal of Heat and Mass Transfer 62 (2013) 495–506.

[31] B. Straughan, Stability and Wave Motion in Porous Media, Springer, New York, 2008.

[32] L. A. Sphaier, A. Barletta, M. Celli, Unstable mixed convection in a heated inclined porous channel, Journal of Fluid Mechanics 778 (2015) 428–450.

[33] K. Atkinson, W. Han, Theoretical Numerical Analysis, 3rd Edition, Springer, New York, 2009.

[34] P. Falsaperla, A. Giacobbe, G. Mulone, Nonlinear stability results for plane Couette and Poiseuille flows, Physical Review E 100 (2019) 013113.

[35] P. Falsaperla, A. Giacobbe, G. Mulone, Inclined convection in a porous Brinkman layer: linear instability and nonlinear stability, Proceedings of the Royal Society A 475 (2019) 20180614.